

**PREPARATION, CHARACTERIZATION AND PHOTOCATALYTIC  
APPLICATIONS OF IMMOBILIZED POLYANILINE COATED TITANIA  
COMPOSITE FOR THE REMOVAL OF DYE AND DIURON FROM  
AQUEOUS SOLUTION**

by

**MOHD FAIRUL SHARIN BIN ABDUL RAZAK**

**Thesis submitted in fulfillment of the requirements for the degree of Doctor of  
Philosophy**

**August 2014**

## ACKNOWLEDGEMENTS

IN THE NAME OF ALLAH, MOST GRACIOUS, MOST MERCIFUL

It would not have been possible to write this doctoral thesis without the help and support of the kind people around me, to only some of whom it is possible to give particular mention here. First and foremost, my utmost gratitude to the one above all of us, the omnipresent only God, for giving me the strength to plod on despite my desire to give up, thank you so much my Allah, I would like to express my deepest gratitude to my supervisor Prof.Dr Mohd Asri Mohd Nawawi for his patience, encouragement, supervision and continuous support. I would also like to extend my thanks to Institut Pengajian Siswazah, Universiti Sains Malaysia and for research funds (Science fund Grant: 227/PKIMIA/821040 and FRGS Grant: 203/PKIMIA/ 843102) from Ministry of Science Technology & Innovation (MOSTI), Malaysia.

Besides that, I acknowledge my sponsorship from the Ministry of Higher Education and Universiti Malaysia Perlis for the Skim Latihan Akademik Bumiputra (SLAB). My gratitude also goes to the administrative and technical staff of School of Chemical Sciences, School of Physics and School of Biological Sciences USM for their assistance throughout my research. I am also indebted to all members of photocatalysis laboratory for their useful suggestions and encouragement. Finally, I would like to express my special gratitude especially to my wife Azliza and daughter Aleesya, my dearest family my mother and sister; Siti Rohani and Laila. For My Parent in Law; Azani Che Din and Zainah for their love, understanding, never ending encouragement and financial support during challenging times for completing my research studies in Universiti Sains Malaysia.

## TABLE OF CONTENTS

	Page
Acknowledgments	ii
Table of Contents	iii
List of Tables	xi
List of Figures	xii
List of Abbreviations	xvii
Abstrak	xix
Abstract	xx
<b>CHAPTER ONE :INTRODUCTION</b>	
1.1 Environmental Problems	1
1.2 Advance Oxidation Processes (AOP)	2
1.3 Heterogeneous Photocatalysis	4
1.4 TiO <sub>2</sub> as a photocatalyst	5
1.4.1 Mechanism of TiO <sub>2</sub> photocatalytic reaction	6
1.4.2 Application of TiO <sub>2</sub>	10
1.5 Strategies for improving TiO <sub>2</sub> photoactivity	12
1.5.1 Self-sensitization by using colored pollutants	12
1.5.2 Dye modified TiO <sub>2</sub>	13
1.5.3 Metal ions modified TiO <sub>2</sub>	14
1.5.4 Doping of TiO <sub>2</sub> with non-metal	14
1.5.5 Doping TiO <sub>2</sub> with conducting polymer	15
1.6 Immobilization of P-25 TiO <sub>2</sub> photocatalyst	16
1.7 ENR/PVC Polymer Blend	17

1.8	Polyaniline (PANI)	19
1.9	Method of PANI synthesis	23
1.9.1	Synthesis of polyaniline colloidal dispersion	23
1.9.2	Direct and inverse emulsion polymerization of aniline	24
1.9.3	Solution polymerization of aniline	25
1.9.4	Interfacial polymerization of aniline	26
1.9.5	Sonochemical synthesis of polyaniline	26
1.9.6	Self-assembling polymerization	27
1.10	Charge Transport in Polyaniline	28
1.11	Applications of Polyaniline	29
1.12	Doping TiO <sub>2</sub> with PANI	31
1.13	The Mechanism of PANI/TiO <sub>2</sub>	33
1.14	Anionic Reactive Red 4 (RR4)	35
1.15	Diuron	36
1.16	Problem statements	38
1.17	Research Objectives	40

## **CHAPTER TWO: MATERIALS AND METHODS**

2.1	Materials and Chemicals	42
2.2	Instruments and equipments	43
2.3	Reactors	
2.3.1	Photoreactor irradiation set up and light sources	44
2.3.2	Adsorption system set up	46

2.4	Preparation of stock solution	
2.4.1	Preparation of Reactive Red 4(RR4) dye solutions	46
2.4.2	Preparation of Diuron solutions	46
2.5	Synthesis of soluble polyaniline	47
2.6	Preparation of epoxidized natural rubber 50 (ENR50) solutions	47
2.6.1	Determination of the ratio of ENR50 to toluene	48
2.7	Preparation of P-25TiO <sub>2</sub> /ENR/PVC formulation	48
2.8	Preparation of P-25TiO <sub>2</sub> /PANI/ENR/PVC coating formulation	49
2.8.1	Optimization of P-25TiO <sub>2</sub> /PANI/ENR/PVC composite loading	49
2.9	Photo-etching of immobilized P-25TiO <sub>2</sub> /PANI/ENR/PVC composite	50
2.10	Characterization of the photocatalyst systems	50
2.10.1	TEM analysis	51
2.10.2	SEM/EDX analysis	51
2.10.3	Elemental analysis (CHNS)	51
2.10.4	FTIR analysis	52
2.10.5	UV-Visible diffuse reflectance spectroscopy (DRS)	52
2.10.6	Photoluminescence spectrum (PLS) analysis	53
2.10.7	TGA analysis	53
2.10.8	BET analysis	54
2.10.9	XPS analysis	54
2.10.10	HRTEM analysis	54
2.11	Photocatalytic degradation of RR4 using P-25TiO <sub>2</sub> /PANI/ENR/PVC	55
2.11.1	Effect of photocatalyst loading on photocatalytic Activity	55

2.11.2	Effect of aeration rates	55
2.11.3	Effect on initial concentration of RR4 on its photocatalytic	56
2.11.4	Effect of initial pH of RR4 dye solutions	56
2.11.5	Determination of point of zero charge (pHpzc) for P-25TiO <sub>2</sub> /PANI/ENR/PVC photocatalyst	56
2.11.6	UV filter analysis	57
2.12	Mineralization study of RR4 and Diuron	57
2.12.1	Preparation of chemical oxygen demand (COD) reagent	57
2.12.2	Chemical oxygen demand (COD)	58
2.12.3	Total organic carbon (TOC)	58
2.12.4	Ion Chromatographic (IC) analysis	59
2.13	Comparison of adhesion properties of P25TiO <sub>2</sub> /ENR/PVC and P-25TiO <sub>2</sub> /PANI/ENR/PVC	60
2.14	The reusability and stability of the photocatalyst systems	60
2.15	Detection of intermediates from photocatalytic degradation of pollutant	
2.15.1	HPLC analysis	61
2.15.2	GC-MS analysis	61
2.15.3	LC-MS analysis	61

**CHAPTER THREE: RESULTS AND DISCUSSION:  
Characterization of synthesized PANI, P-25TiO<sub>2</sub>/PANI/ENR/PVC  
and P-25TiO<sub>2</sub>/ENR/PVC system**

3.1	Introduction	63
3.2	Physical Characterisation of Synthesized PANI	64
3.2.1	Conductivity Measurement	64
3.2.2	Elemental analysis	65

3.2.3	FTIR analysis	66
3.2.4	Raman analysis	68
3.2.5	Diffuse Reflectance Spectra Study	69
3.2.6	TGA analysis	70
3.2.7	TEM and SEM analyses	73
3.2.8	BET analysis	75
3.2.9	PL analysis	75
3.3	Physical Characterization of P-25TiO <sub>2</sub> /PANI/ENR/PVC Composite	77
3.3.1	FTIR analysis	77
3.3.2	Raman study	79
3.3.3	UV-Vis Diffused Reflectance Spectra (UV-Vis DRS) Analysis	81
3.3.4	PL analysis	82
3.3.5	SEM analysis	84
3.3.6	TGA analysis	86
3.3.7	X-ray Photoelectron Spectroscopy (XPS) analysis	91
3.4	Characterization of P25 TiO <sub>2</sub> /PANI/ENR/PVC at different volume ratio TiO <sub>2</sub> :PANI	94
3.4.1	UV-Vis Diffused Reflectance Spectra (UV-Vis DRS) analysis	96
3.4.2	PL study	97
3.4.3	SEM analysis	99
3.4.4	HRTEM analysis	101
3.5	Adhesion strength test	103

**CHAPTER FOUR: RESULT AND DISCUSSION:  
Photocatalytic degradation of RR4 by P-25TiO<sub>2</sub>/PANI/ENR/PVC and  
P-25TiO<sub>2</sub>/ENR/PVC system**

4.1	Introduction	104
4.2	Photocatalytic Degradation of RR4 Dye by immobilized P-25 TiO <sub>2</sub> /PANI/ENR/PVC	105
4.2.1	Comparison of photocatalytic activity of a preliminary PANI doped TiO <sub>2</sub> with TiO <sub>2</sub> slurry system	105
4.2.2	Optimization of PANI:TiO <sub>2</sub> ratio for the photocatalytic degradation of RR4 dye	107
4.3	The Operational Parameters Governing the Photocatalytic Degradation of RR4 by P-25TiO <sub>2</sub> /PANI/ENR/PVC Photocatalyst system	109
4.3.1	The effect of catalyst loading	109
4.3.2	The effect of initial concentration	111
4.3.3	The effect of pH solutionS	113
4.3.4	The effect of aeration rate	116
4.4	Intermediates of RR4 dye during its photocatalytic degradation	119
4.5	Mineralization study	122
4.5.1	Detection of anion compounds (SO <sub>4</sub> <sup>2-</sup> , NO <sub>3</sub> <sup>-</sup> and Cl <sup>-</sup> )	124

**CHAPTER FIVE: RESULTS AND DISCUSSION:  
Effect of pre-irradiation of immobilized P-25TiO<sub>2</sub>/PANI/ENR/PVC**

5.1	Introduction	126
5.2	Optimization of the time of pre-irradiation	127
5.2.1	COD analysis	127
5.3	Characterization of P-25TiO <sub>2</sub> /PANI/ENR/PVC-7hr	129
5.3.1	BET and EDX analyses	129
5.3.2	FTIR analysis	131



5.3.3	Raman and (UV-Vis DRS) analyses	133
5.3.4	TGA analysis	135
5.3.5	PL analysis	137
5.3.6	SEM analysis	138
5.3.7	HRTEM analysis	140
5.4	Photocatalytic activity of P-25TiO <sub>2</sub> /PANI/ENR/PVC/(1:0.0035)-7h	141
5.5	Mineralization study	143
5.6	Visible light response	145
5.7	Reusability of the immobilized system	147

## **CHAPTER SIX: RESULTS AND DISCUSSION:**

### **Photocatalytic degradation of diuron using immobilized P-25 TiO<sub>2</sub>/PANI/ENR/PVC (1:0.0035)-7h**

6.1	Introduction	149
6.2	Comparison of percentage removal of Diuron under different photocatalytic systems	150
6.2.1	Photocatalysis and adsorption study	153
6.3	The Operational Parameters Governing the Photocatalytic Degradation of Diuron Solution by P-25TiO <sub>2</sub> /PANI/ENR/PVC (1:0.0035)-7h Photocatalyst system	154
6.3.1	Effect of Concentration	154
6.3.2	Effect of Initial pH of diuron solution	156
6.4	Identification of intermediates	158
6.4.1	HPLC study	158
6.4.2	LCMS study	160

6.5	Mineralization study	162
	6.5.1 Detection of ions ( $\text{NO}_3^-$ and $\text{Cl}^-$ )	162
	6.5.2 TOC study	164
<b>CHAPTER SEVEN: CONCLUSIONS</b>		
7.1	Conclusions	166
<b>REFERENCES</b>		169
<b>APPENDICES</b>		186
<b>LIST OF PUBLICATIONS AND CONFERENCES</b>		191

## LIST OF TABLES

		Page
Table 1.1:	Chemical structures of typical conjugated polymers	20
Table 1.2:	The colors of each oxidation state of PANI.	21
Table 3.1:	The resistivity and conductivity values of protonated PANI and PANI EB	64
Table 3.2:	Elemental content of synthesized protonated PANI and PANI EB.	65
Table 3.3:	Thermogravimetric data of P-25TiO <sub>2</sub> /ENR/PVC, and P-25TiO <sub>2</sub> /PANI/ENR/PVC at different TiO <sub>2</sub> : PANI ratios before and after irradiation.	90
Table 3.4	The calculated band gap energies of composites at different amount of PANI dopant using the Kubelca Mulk method.	97
Table 4.1:	The pseudo first order rate constant for the degradation of RR4 dye by P-25TiO <sub>2</sub> slurry, immobilized P-25 TiO <sub>2</sub> /ENR/PVC and at different volume ratio TiO <sub>2</sub> /PANI.	108
Table 4.2:	The calculated rate constant of RR4 dye at different initial concentration	112
Table 4.3:	Point of zero charge (pH <sub>pzc</sub> ) for p-25 powder and the immobilized P-25/PANI/ENR/PVC	114
Table 5.1:	The percentage of carbon content based on etching time from 0 to 7 hours of irradiation and the surface area (BET) before and after 7 hours of irradiation.	130
Table 6.1:	The pseudo first order rate constant for the photocatalytic degradation of diuron by immobilized P-25 TiO <sub>2</sub> /PANI/ENR/PVC (1:0.0035)-7h, P-25TiO <sub>2</sub> /PANI/ENR/PVC (1:00035 P-25TiO <sub>2</sub> /ENR/PVC and P-25TiO <sub>2</sub> slurry.	151
Table 6.2:	The calculated rate constant of diuron by using formula first order reaction.	155
Table 6.3:	Identified intermediates compounds for the degradation of diuron by P-25TiO <sub>2</sub> /PAN/ENR/PVC(1.0035)-7h.	160

## LIST OF FIGURES

	Page
Figure 1.1: Main methods used for the removal of organic dyes from wastewaters (Martínez-Huitle and Brillas, 2009).	3
Figure 1.2: Crystalline structures of titanium dioxide (a) anatase, (b) rutile, (c) brookite (Pelaez et al., 2012).	5
Figure 1.3: Schematic of semiconductor excitation by band gap illumination (Ibhadon and Fitzpatrick, 2013).	7
Figure 1.4: Applications of TiO <sub>2</sub> (Nakata et al., 2012).	11
Figure 1.5: The general structure of (a) PANI and (b) The chemical structures of four oxidation states of polyaniline (Sharma, 2006).	22
Figure 1.6: Schematic illustration of a negative soliton (a) and (c) moving along the polymer chain and neutral state soliton (b) and (d) (Frohne, 2004).	29
Figure 1.7: Mechanism of photodegradation of organic contaminants by PANI/TiO <sub>2</sub> photocatalyst under visible light irradiation (solid line) and under UV light irradiation (dotted line) (Singh et al., 2013).	34
Figure 1.8: Molecular structure of RR4 dye.	35
Figure 1.9: Molecular structure of Diuron.	36
Figure 1.10: Environmental impact of pesticides (2013), [online], [accessed 13 July 2013]. Available from Wikipedia, the free encyclopedia. <a href="http://en.wikipedia.org/wiki/">http://en.wikipedia.org/wiki/</a>	37
Figure 2.1 (A-B): The photocatalytic experimental set up for the degradation and mineralization study of RR4 azo dye; (a) homemade photoreactor with target pollutant, (b) 45-Watt fluorescent Lamp (c) Aeration inlet using pipette, (d) Immobilized plate PANI/TiO <sub>2</sub> /ENR/PVC(e) scissor jack and (f) power supply connection.	45
Figure 3.1: FTIR spectras of (a) protonated PANI (b) PANI EB.	67
Figure 3.2: Raman spectra of protonated PANI.	68

Figure 3.3:	Diffuse reflectance spectra of (a) PANI EB; (b) protonated PANI	70
Figure 3.4:	The thermogravimetric of (a) protonated PANI and (b) commercial PANI EB.	72
Figure 3.5:	TEM micrograph of soluble PANI (a); Scanning electron micrograph of the surface of synthesized PANI at different spot (b-c) and (d) Scanning electron micrograph of commercial PANI EB.	74
Figure 3.6:	PL spectra of (a) protonated PANI and (b) PANI EB.	76
Figure 3.7:	The FTIR spectra of (a) Pristine P-25TiO <sub>2</sub> (b) P-25TiO <sub>2</sub> /ENR/PVC and (c) P-25TiO <sub>2</sub> /PANI/ENR/PVC.	78
Figure 3.8:	Raman spectra of (a) PANI (i), P-25TiO <sub>2</sub> /ENR/PVC (ii), P-25 TiO <sub>2</sub> /PANI/ENR/PVC/0 hrs (iii) and (b) PVC (i) and ENR (ii).	80
Figure 3.9:	DRS spectras of (a) PANI, (b) P-25TiO <sub>2</sub> /PANI/ENR/PVC and (c) P-25TiO <sub>2</sub> /ENR/PVC.	81
Figure 3.10:	PL spectrum of (a) P25 TiO <sub>2</sub> powder (b) P-25TiO <sub>2</sub> /ENR/PVC and (c) P-25TiO <sub>2</sub> /PANI/ENR/PVC.	83
Figure 3.11:	Scanning electron micrograph (a) P-25 powder, (b) P-25 TiO <sub>2</sub> /ENR/PVC and (c) P-25 TiO <sub>2</sub> /PANI/ENR/PVC.	85
Figure 3.12:	TG and DTG profile (a) of P-25 TiO <sub>2</sub> /ENR/PVC, and (b) P- 25TiO <sub>2</sub> /PANI/ENR/PVC.	88
Figure 3.13:	TG profile of P-25TiO <sub>2</sub> /PANI/ENR/PVC at different volume TiO <sub>2</sub> :PANI ratio.	89
Figure 3.14:	XPS spectra of (a) the survey spectrum, (b) C1s (c) O1s and (d) N1s for the P-25TiO <sub>2</sub> /PANI/ENR/PVC (1:0.0035).	93
Figure 3.15a:	DRS spectra of (i) PANI powder , at different volume ratio TiO <sub>2</sub> :PANI;(ii)P25TiO <sub>2</sub> /PANI/ENR/PVC(1:0.0057);(iii) P25TiO <sub>2</sub> /PANI/ENR/PVC(1:0.0043);(iv)P25TiO <sub>2</sub> /PANI /ENR/PVC(1:0.0035);(v)P25TiO <sub>2</sub> /PANI/ENR/PVC(1:0.0028);(vi)P-25TiO <sub>2</sub> /ENR/PVC.	96
Figure 3.15b:	The band gap of the samples determined by using Kubelka Munk method	96

Figure 3.16:	Photoluminescence spectra of (a) P-25 TiO <sub>2</sub> /ENR/PVC, (b) P-25 TiO <sub>2</sub> /PANI/ENR/PVC (1:0.0057), (c) P-25 TiO <sub>2</sub> /PANI/ENR/PVC(1:0.0043), (d) P-25 TiO <sub>2</sub> /PANI/ENR/PVC (1:0.0028) and (e) P-25 TiO <sub>2</sub> /PANI/ENR/PVC (1:0.0035).	98
Figure 3.17:	SEM micrographs of (a) P-25 TiO <sub>2</sub> /PANI/ENR/PVC (1:0.0028), (b) P-25 TiO <sub>2</sub> /PANI/ENR/PVC(1:0.0035), (c) P-25 TiO <sub>2</sub> /PANI/ENR/PVC(1:0.0043) and (d) P-25 TiO <sub>2</sub> /PANI/ENR/PVC(1:0.0057).	100
Figure 3.18:	TEM micrographs of (a) P-25TiO <sub>2</sub> /PANI/ENR/PVC(1:0.0035), (b) P-25TiO <sub>2</sub> /ENR/PVC; HRTEM of (c) P-25TiO <sub>2</sub> /PANI/ENR/PVC(1:0.0035) and (d) P-25 TiO <sub>2</sub> /ENR/PVC (1:0.0057).	102
Figure 3.19:	A comparison of adhesion strength of immobilized P-25TiO <sub>2</sub> /ENR/PVC and P-25TiO <sub>2</sub> /PANI/ENR/PVC on glass plates via the sonication test.	103
Figure 4.1:	Percentage of the remaining of RR4 dye due to the photolysis and photocatalytic degradation by P-25TiO <sub>2</sub> suspension, and immobilized P-25TiO <sub>2</sub> /ENR/PVC and P-25 TiO <sub>2</sub> /PANI/ENR/PVC.	106
Figure 4.2:	Photocatalytic degradation of 30 mg L <sup>-1</sup> RR4 dye under a 45-W fluorescent lamp by immobilized P-25 TiO <sub>2</sub> /ENR/PVC, TiO <sub>2</sub> slurry and immobilized P-25TiO <sub>2</sub> /PANI/ENR/PVC at different volume ratio TiO <sub>2</sub> /PANI.	108
Figure 4.3:	The pseudo first order rate constant of the photocatalytic degradation of RR4 dye by (a) P-25TiO <sub>2</sub> /PANI/ENR/PVC (1:0.0035); (b) P-25TiO <sub>2</sub> /ENR/PVC and adsorption of RR4 dye by (c) P-25TiO <sub>2</sub> /PANI/ENR/PVC and (d) adsorption of P-25TiO <sub>2</sub> /ENR/PVC.	110
Figure 4.4:	The pseudo first order rate constant of the photocatalytic degradation of RR4 dye at different initial concentration by the optimized PANI coated P-25 TiO <sub>2</sub> /PANI/ENR/PVC (1:0.0035) catalyst plate.	112
Figure 4.5:	The pseudo first order rate constant of RR4 dye at different initial pH values by P-25TiO <sub>2</sub> /PANI/ENR/PVC(1:0.0035) catalyst plate.	115

Figure 4.6:	The first order rate constants of RR4 dye at different aeration flow rate by using P-25TiO <sub>2</sub> /PANI/ENR/PVC(1:0.0035) system.	118
Figure 4.7:	HPLC chromatograms of (a) initial RR4 (b) intermediates from its photocatalytic degradation.	120
Figure 4.8:	The proposed mechanism of the photo degradation of RR4 by P-25.	121
Figure 4.9:	COD removal of RR4 solution by photocatalytic process using P-25TiO <sub>2</sub> /PANI/ENR/PVC(1:0.0035) and P-25TiO <sub>2</sub> /ENR/PVC.	123
Figure 4.10:	Evolution of inorganic ions from the photocatalytic degradation of RR4 dye by immobilized P-25TiO <sub>2</sub> /PANI/ENR/PVC (1:0.0035).	125
Figure 5.1:	COD values of the irradiated water in the present of the immobilized P-25TiO <sub>2</sub> /PANI/ENR/PVC(1:0.0035) representing leachable organic from the irradiated plate.	128
Figure 5.2:	The nitrogen adsorption-desorption isotherms for P-25TiO <sub>2</sub> /PANI/ENR/PVC (1:0.0035)-7h.	130
Figure 5.3:	The FTIR spectrum of P-25TiO <sub>2</sub> /PANI/ENR/PVC (1:0.0035) after 7hours of irradiation.	132
Figure 5.4A:	Raman spectra for (a) P-25TiO <sub>2</sub> /PANI/ENR/PVC(1:0.0035)-7h (b) P-25TiO <sub>2</sub> /PANI/ENR/PVC(1:0.0035)	134
Figure 5.4B:	DRS spectra of P-25TiO <sub>2</sub> /PANI/ENR/PVC(1:0.0035)-7h.	134
Figure 5.5:	The TGA thermograms of (a) P-25TiO <sub>2</sub> /ENR/PVC-5h and P-25TiO <sub>2</sub> /PANI/ENR/PVC-5h.	136
Figure 5.6:	The PL spectra of (a) P-25TiO <sub>2</sub> /PANI/ENR/PVC(1:0.0035) and (b) P-25TiO <sub>2</sub> /PANI/ENR/PVC (1:0.0035)-7h.	137
Figure 5.7:	SEM micrographs of P-25TiO <sub>2</sub> /PANI/ENR/PVC (1:0.0035) at 5K magnification (a) before irradiation and (b) after 7 h of irradiation.	139

Figure 5.8:	The HRTEM micrograph of P-25TiO <sub>2</sub> /PANI/ENR/PVC-7h.	140
Figure 5.9:	Photocatalytic degradation of 30 mg L <sup>-1</sup> RR4 dye at (a) difference systems condition and (b) pseudo first order rate constants for the degradation of RR4 dye via photocatalysis and adsorption processes using (1) P-25TiO <sub>2</sub> /ENR/PVC, (2) P-25TiO <sub>2</sub> /ENR/PVC-7hr,(3)P-25TiO <sub>2</sub> /PANI/ENR/PVC(1:0.0035) and (4) P-25TiO <sub>2</sub> /PANI/ENR/PVC (1:0.0035)-7hr.	142
Figure 5.10:	The COD value for the photocatalytic degradation of 60 mg L <sup>-1</sup> RR4 dye by P-25TiO <sub>2</sub> /ENR/PVC/7h and P-25TiO <sub>2</sub> /PANI/ENR/PVC/7h.	144
Figure 5.11:	Photocatalytic degradation of 30 mg L <sup>-1</sup> RR4 dye under visible light irradiation by various photocatalyst systems: (a) TiO <sub>2</sub> slurry, UV filtered; (b) P-25TiO <sub>2</sub> /PANI/ENR/PVC (1:0.0035); (c) P-25TiO <sub>2</sub> /PANI/ENR/PVC(1:0.0035)-7h; d) P-25TiO <sub>2</sub> /ENR/PVC-7h and (e) P-25TiO <sub>2</sub> slurry.	146
Figure 5.12:	The pseudo first order rate constants for the photocatalytic degradation of RR4 dye up to 10 recycled applications using different immobilized plate system namely P-25TiO <sub>2</sub> /ENR/PVC-7h, P-25TiO <sub>2</sub> /PANI/ENR/PVC(1:0.0035)-7h and P-25TiO <sub>2</sub> /PANI/ENR/PVC(1:0.0035).	148
Figure 6.1:	The adsorption of diuron by different photocatalyst systems.	152
Figure 6.2:	Photocatalytic degradation of diuron under a 45-W fluorescent lamp using various photocatalyst systems.	153
Figure 6.3:	The effect of initial concentration on the photocatalytic degradation of diuron by using P-25TiO <sub>2</sub> /PANI/ENR/PVC (1:0.0035)-7h catalyst plate.	155
Figure 6.4:	The pseudo first order rate constant for photocatalytic degradation of diuron at different initial pH values by using P-25TiO <sub>2</sub> /PANI/ENR/PVC (1:0.0035)-7h catalyst plate.	157
Figure 6.5:	HPLC chromatograms of (a) initial diuron, (b) after 1 h of irradiation and (c) 2 h of irradiation.	159
Figure 6.6:	The proposed mechanism of the degradation of diuron after 2 h of irradiation.	161



Figure 6.7:	Evolution of inorganic ions from the photocatalytic degradation of diuron by immobilized P-2TiO <sub>2</sub> /PANI/ENR/PVC(1:0.0035)-7h.	163
Figure 6.8:	TOC values for the photocatalytic degradation of 10 mg L <sup>-1</sup> diuron by using P-25TiO <sub>2</sub> /PANI/ENR/PVC (1:0.0035)-7h system.	165

## LIST OF ABBREVIATIONS

AOPs	Advance oxidation processes
APS	Ammonium persulfate
a.u	Arbitrary units
BQET	benzenoid-to-quinoid excitonic transition
CB	Conduction Band
CHNS	Carbon, Hydrogen Nitrogen Sulfur
COD	Chemical Oxygen Demand
CPs	Conjugated Polymers
$e^-$	Negative electron
$E_{bg}$	Energy band gap
ENR50	Epoxidized natural rubber 50
ES	Emeraldine salt
ESD	Electrostatic discharge
EMI	Electromagnetic interference shielding
$\lambda_{ex}$	Excitation wavelengths
$\lambda_{max}$	Lambda maximum
$H_2O_2$	Hydrogen peroxide
$h^+$	Positive hole
$h\nu$	Photonic energy
HOMO	Highest unoccupied molecular orbital
HPLC	High Performance Liquid Chromatography
HRTEM	High Resolution Transmission Electron Microscopy
ICPs	Ionic conducting polymers
ITO	indium tin oxide
LUMO	lowest unoccupied molecular orbital
MSAN	m-aminobenzene sulfonic acid
NHE	Normal hydrogen electrode
$O_3$	Ozone
PANI	Polyaniline
PANI EB	Polyaniline emeraldine base
PANI-ES	Polyaniline emeraldine salt
PL	Photoluminescence
PET	Polyethylene terephthalate
PI	Polyimide
PS	Polystyrene
PVC	Polyvinyl chloride
PVP	Poly(N-vinylpyrrolidone)
pzc	Point of zero charge
RR4	Reactive Red 4 dye
SEM	Scanning Electron Microscopy

$S_{\text{BET}}$	Surface area BET
TIPP	Titanium tetraisopropoxide
TOC	Total organic carbon
TOC/TOC <sub>0</sub>	Remaining organic carbon divided by initial total organic
UV	Ultra violet
UV-VIS DRS	UV-Visible diffuse reflectance spectroscopy
VB	Valence band
XPS	X-ray photoelectron spectroscopy

**PENYEDIAAN, PENCIRIAN DAN APLIKASI FOTOPEMANGKINAN  
KOMPOSIT TERPEGUN TITANIA BERSALUT PANI BAGI  
PENYINGKIRAN PENCELUP WARNA DAN DIURON DARIPADA  
LARUTAN AKUEUS**

**ABSTRAK**

Fotomangkin P-25TiO<sub>2</sub>/PANI/ENR/PVC telah berjaya dihasilkan dan dipegunkan pada plat kaca melalui kaedah penyaduran celup. Ampaian penyaduran celup telah disediakan oleh pencampuran ringkas PANI terlarut dengan serbuk P-25TiO<sub>2</sub> dalam pelarut diklorometana-toluena yang mengandungi getah asli terepoksi (ENR) dan polyvinilklorida (PVC) yang berfungsi sebagai ejen pengikat. Kemasukan PANI terlarut ke dalam ampaian P-25 telah mengukuhkan kekuatan lekatan plat yang dihasilkan. Kehadiran PANI dalam ampaian P-25 telah mengurangkan intensiti PL yang menunjukkan bahawa penggabungan semula elektron-lubang adalah rendah. Tambahan pula, gerakbalas foto P-25TiO<sub>2</sub>/PANI/ENR/PVC telah dilanjutkan kepada kawasan cahaya nampak yang pada masa yang sama telah meningkatkan fotoaktiviti komposit masing-masing. Nilai tenaga luang jalur untuk P-25TiO<sub>2</sub>/PANI/ENR/PVC komposit optimum (1:0.0035) adalah 2.86 eV di mana polianalina (PANI) membentuk lapisan kulit teras kira-kira 0.9 nm dengan interaksi PANI-TiO<sub>2</sub> yang kuat. Dengan menggunakan pencelup warna reaktif merah 4 (RR4) dan herbisida diuron, sebagai model bahan pencemar, fotoaktiviti kompos optimum P-25TiO<sub>2</sub>/PANI/ENR/PVC(1:0.0035) adalah 2.8 dan 2 kali lebih cepat daripada sistem pegun P-25TiO<sub>2</sub>/ENR/PVC. Seperti yang diperhatikan, kadar pemineralan kedua-dua bahan pencemar telah bertambah baik dan laluan penguraian mekanisme masing-masing telah dicadangkan. Menariknya, pra-penyinaran pegun P-

25TiO<sub>2</sub>/PANI/ENR/PVC(1:0.0035) komposit selama 7 j telah menambahbaik sistem aktiviti fotopemangkinan di mana kadar penguraian RR4 hampir sama dengan sistem TiO<sub>2</sub> terampai. Malahan fotopenguraian diuron adalah lebih berkesan daripada sistem terampai dengan menggunakan keadaan ini. Selain itu, P-25TiO<sub>2</sub>/PANI/ENR/PVC(1:0.0035)-7j adalah bersifat sensitif cahaya nampak di mana 85 % daripada 30 mg L<sup>-1</sup> pencelup warna RR4 dinyahwarna selepas 60 minit sinaran cahaya. Kedua-dua P-25TiO<sub>2</sub>/PANI/ENR/PVC terpegun (1:0.0035)-7j dan fotomangkin P-25TiO<sub>2</sub>/ENR/PVC-7j sangat boleh diulang guna dan bersifat mampan dengan nilai pseudo kadar tertib pertama bagi fotopengurai RR4 adalah  $0.103 \pm 0.002 \text{ min}^{-1}$  dan  $0.066 \pm 0.001 \text{ min}^{-1}$ .

**PREPARATION, CHARACTERIZATION AND PHOTOCATALYTIC  
APPLICATIONS OF IMMOBILIZED PANI COATED TITANIA  
COMPOSITE FOR THE REMOVAL OF DYE AND DIURON FROM  
AQUEOUS SOLUTION**

**ABSTRACT**

P-25TiO<sub>2</sub>/PANI/ENR/PVC composite photocatalyst has been successfully fabricated and immobilized onto glass plates via a dip coating method. Dip coating dispersion was prepared by simple mixing of soluble polyaniline (PANI) with P-25TiO<sub>2</sub> powder in the dichloromethane-toluene solvent containing epoxidized natural rubber (ENR) and polyvinylchloride (PVC) which function as binding agents. Inclusion of soluble PANI into P-25 dispersion had strengthened the adhesion of the fabricated photocatalyst plate. The present of PANI in the P-25 dispersion had also reduced the PL intensity indicating the lower effect of electron-hole recombination. Additionally, the photoresponse of P-25TiO<sub>2</sub>/PANI/ENR/PVC was extended into the visible light region which simultaneously improved the photoactivity of the composite respectively. The band gap energy of the optimum composite P-25TiO<sub>2</sub>/PANI/ENR/PVC (1:0.0035) was 2.86 eV where PANI formed a core shell coating of about 0.9 nm with a strong PANI-TiO<sub>2</sub> interaction. Based on reactive red 4 (RR4) dye and diuron as model pollutants, the photocatalytic activity of the optimum P-25TiO<sub>2</sub>/PANI/ENR/PVC (1:0.0035) composite was 2.8 and 2 fold faster than the immobilized P-25TiO<sub>2</sub>/ENR/PVC system. As observed, the mineralization rates of both pollutants were improved and the degradation mechanism pathways were proposed respectively. Interestingly, pre-irradiation of the immobilized P-25TiO<sub>2</sub>/PANI/ENR/PVC (1:0.0035) composite for 7 h improved the photocatalytic

activity of the system whereby degradation rate of RR4 was nearly as same as the TiO<sub>2</sub> suspended system. In fact the photodegradation of diuron was more effective than suspended photocatalytic system under similar conditions. Moreover, P-25TiO<sub>2</sub>/PANI/ENR/PVC(1:0.0035)-7h was visible light sensitive where 85 % of 30 mg L<sup>-1</sup> RR4 dye was decolorized after 60 minutes of irradiation. Both the immobilized P-25TiO<sub>2</sub>/PANI/ENR/PVC(1:0.0035)-7h and P-25TiO<sub>2</sub>/ENR/PVC-7h photocatalyst systems were highly reusable and sustainable with pseudo first order rate constant values of  $0.103 \pm 0.002 \text{ min}^{-1}$  and  $0.066 \pm 0.001 \text{ min}^{-1}$  respectively.

## CHAPTER ONE

### INTRODUCTION

#### 1.1 Environmental Problems

Nowadays, the concern of environmental remediation works has increased day by day due to air, water and solid waste pollutions which contribute a major share to the overall imbalance of the ecosystem. The common pollutants may include toxic chlorinated and non-chlorinated aliphatic and aromatic organic compounds, heavy metals, dyes and agro wastes such as insecticides and herbicides. Organic dyes are one of the largest groups of pollutants released into wastewaters from the textile and other industrial processes (Sharma, 2006; Han et al., 2009). These dyes contain harmful substances and highly toxic which need to be treated by using specific treatment methods for converting such coloured effluents to harmless compounds. Many conventional methods have been proposed to treat these effluents. However each method had its own drawbacks and weaknesses. Conventional oxidation treatments have difficulty to oxidize dyestuffs and complex structures of organic compounds even at low concentrations especially if they are refractory to the oxidants. In the last decade, advanced oxidation processes (AOPs) have been shown to be effective for the destruction of these pollutants via the generation of free hydroxyl radicals. Therefore advanced oxidation processes (AOPs) have been developed to generate hydroxyl free radicals by different techniques. Photocatalytic degradation of pollutants using semiconductors such as  $\text{TiO}_2$  is one of those promising techniques.



## 1.2 Advanced Oxidation Processes (AOPs)

The goal of any AOPs is to generate and use hydroxyl free radical ( $\text{OH}^\bullet$ ) as a strong oxidant to destroy compounds that cannot be oxidized by the conventional oxidant. AOPs are capable of converting hazardous materials in wastewater effluents into water and carbon dioxide, or otherwise, into other innocuous by products. Martínez-Huitle and Brillas,(2009) reported that AOP was one of the main method used for the removal of organic dyes from wastewaters as being shown in Figure 1.1. Major types of AOPs include the employment of ultra violet (UV) light, hydrogen peroxide ( $\text{H}_2\text{O}_2$ ), ozone ( $\text{O}_3$ ), vacuum and semiconductors such as titanium dioxide ( $\text{TiO}_2$ ). Despite of the availability of various AOPs processes, heterogeneous photocatalysis appears to be more effective and popular due to several advantages. The main advantages of heterogeneous photocatalysis are as follows:

- i) Oxidation processes under heterogeneous photocatalysis are capable of mineralizing wide ranges of persistent pollutants unselectively, including reduction of metal ions.
- ii) Photocatalysts are reusable and many ongoing studies are conducted to improve the reproducibility of the catalyst for long term use.
- iii) Semiconductors for the applications of photocatalysis are easily acquired and relatively inexpensive.
- iv) Water treatment via this method can be operated under the illumination of solar light as the photocatalyst can be stimulated under visible light source.

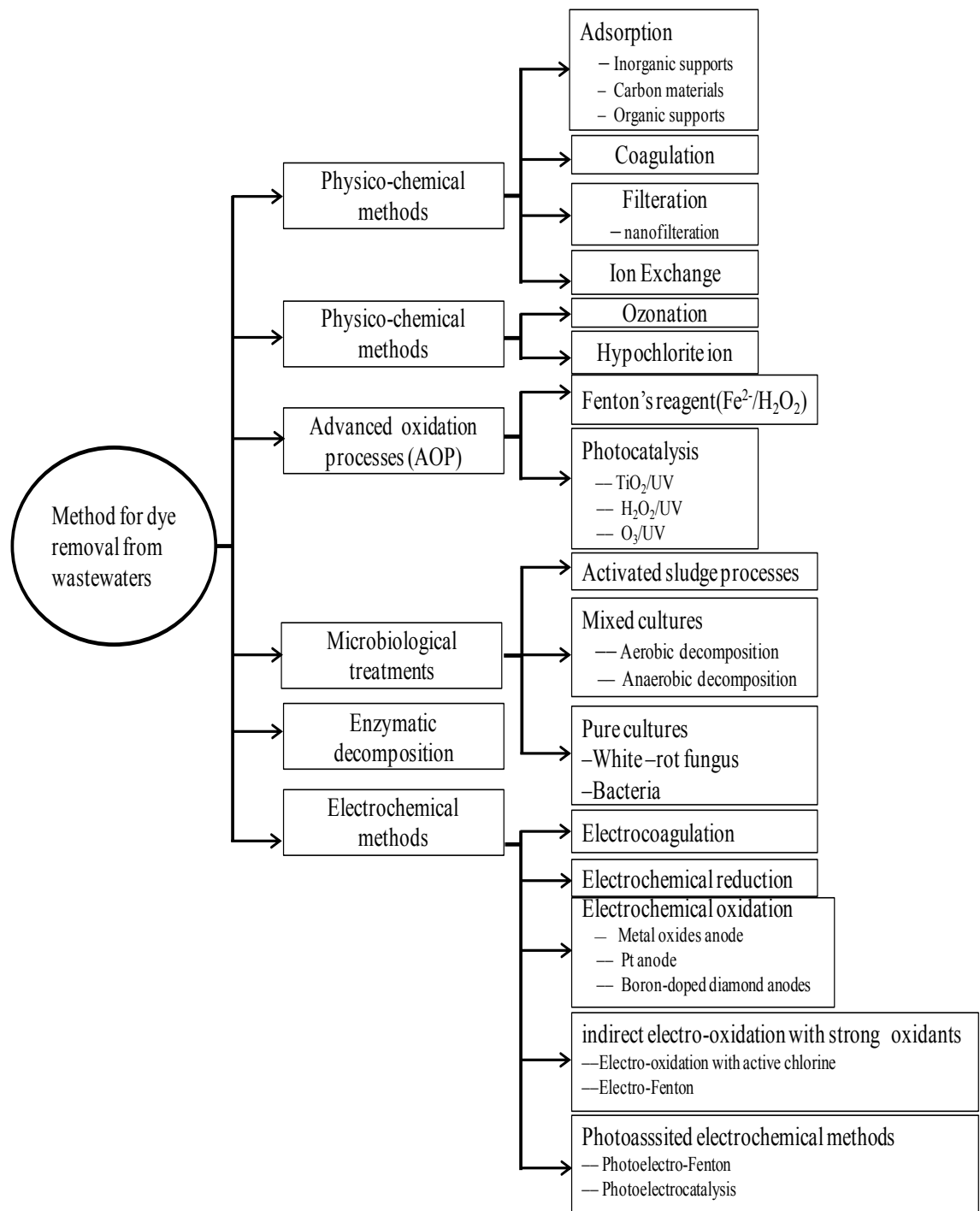


**Figure 1.1** Main methods used for the removal of organic dyes from wastewaters (Martínez-Huitle and Brillas, 2009).

### 1.3 Heterogeneous Photocatalysis

Heterogeneous photocatalysis can be described as the acceleration of photoreactions in the presence of a catalyst in a different phase from the reactants. Heterogeneous photocatalysis is a discipline which includes a large variety of reactions such as mild or total oxidations, dehydrogenation, hydrogen transfer, isotope oxygen-18 to isotope oxygen-16 and deuterium-alkane isotopic exchange, metal deposition, and water detoxification (Herrmann, 1999). Heterogeneous photocatalysis can be carried out in various media such as gas phase and pure organic liquid phases or aqueous solutions. As for classical heterogeneous catalysis, the overall process can be decomposed into five independent steps:

- i. Transfer of the reactants in the fluid phase to the surface
- ii. Adsorption of a least one of the reactants
- iii. Reaction in the adsorbed phase
- iv. Desorption of the products
- v. Removal of the products from the interface region

Exposing the photocatalyst to light with a higher energy than its band gap energy generates excited states in the photocatalyst that are able to initiate oxidation and reduction reactions, thereby forming molecular transformations. Recent research (Nagaveni et al., 2004; Teh and Mohamed, 2011; Pirkanniemi and Sillanpää, 2002; Wodka et al., 2010) shows that TiO<sub>2</sub> based heterogeneous photocatalytic oxidation technologies are still the most promising methods because of its high photoactivity, low cost, low toxicity and good chemical and thermal stability.

## 1.4 TiO<sub>2</sub> as a photocatalyst

Titanium dioxide (TiO<sub>2</sub>) exists in three different polymorphs; anatase, rutile and brookite (Pelaez et al., 2012). The primary source and the most stable form of TiO<sub>2</sub> is rutile. All three polymorphs can be readily synthesised in the laboratory and typically the metastable anatase and brookite will transform to the thermodynamically stable rutile upon calcination at temperatures exceeding 600 °C (Hu et al., 2003a). In all three forms, titanium (Ti<sup>4+</sup>) atoms are co-ordinated to six oxygen (O<sup>2-</sup>) atoms, forming TiO<sub>6</sub> octahedra. Anatase is made up of corner (vertice) sharing octahedra which form (001) planes (Figure 1.2a) resulting in a tetragonal structure. In rutile, the octahedra share edges at (001) planes to give a tetragonal structure (Figure 1.2b), and in brookite both edges and corners are shared to give an orthorhombic structure (Figure 1.2c) (Hu et al.,2003a; Carp et al., 2004 ). Titanium dioxide is typically an n-type semiconductor due to the existence of oxygen deficiency (Wisitsoraat et al., 2009).

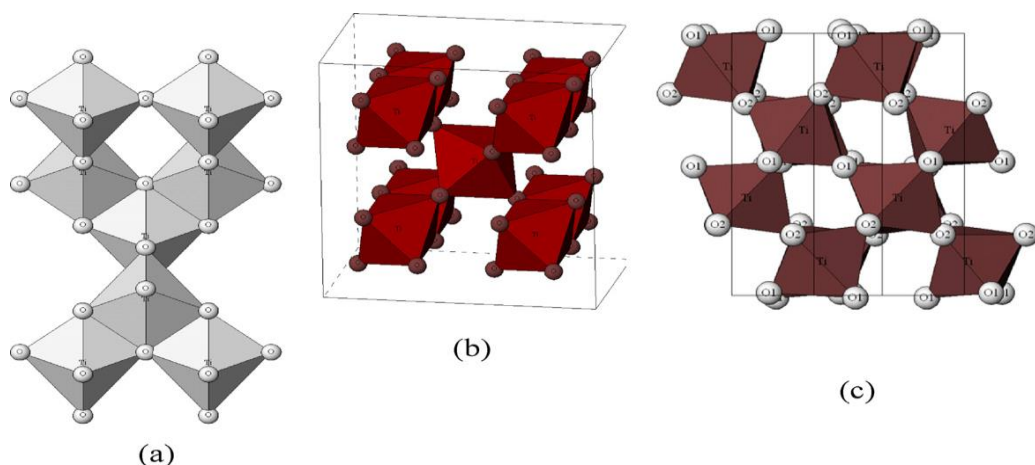


**Figure 1.2:** Crystalline structures of titanium dioxide (a) anatase, (b) rutile, (c) brookite (Pelaez et al., 2012).

Among the various kinds of TiO<sub>2</sub> that are commercially available, Degussa P25 is extensively used in the photocatalytic treatment of water and wastewater. P25 powder, composing of 80 % anatase and 20 % rutile, is widely studied and well known to have a substantially higher photocatalytic activity than most of the other available samples of TiO<sub>2</sub> (Ohno et al., 2001). The first extensive work to correlate the photocatalytic activity and the structure of P25 was carried out by Bickley et al.,(1991). Many researchers attribute the high photocatalytic activity of this photocatalyst to the contact between two phases which enhance the separation of photogenerated electrons and holes, and resulting in their reduced recombination (Yu et al., 2006). Therefore P25 has been chosen as a standard TiO<sub>2</sub> for photocatalytic processes.

#### **1.4.1 Mechanism of TiO<sub>2</sub> in photocatalytic reactions**

Figure 1.3 shows the semiconductor excitation by band gap illumination. Band gap excitation of TiO<sub>2</sub> causes charge separation which is followed by scavenging of electrons and holes by the surface adsorbed species. However, due to its relatively high band gap energy of 3.2 eV, the photocatalytic responses of TiO<sub>2</sub> only work at wavelength <380 nm. The series of chain oxidative-reductive reactions (Equations (1.2) – (1.12)) that take place at the photoinduced TiO<sub>2</sub> surface is generally proposed as follows (Chong et al., 2010):

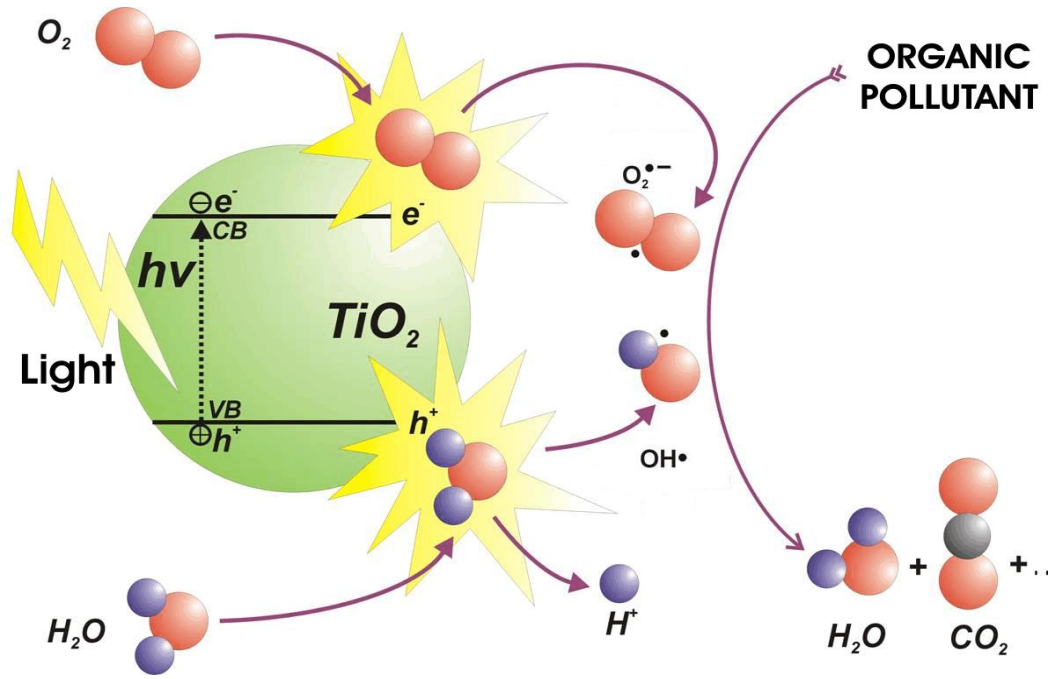


**Figure 1.3:** Schematic of semiconductor excitation by band gap illumination (Ibhadon and Fitzpatrick, 2013).

Photoexcitation :



Charge-carrier trapping of e<sup>-</sup> :



Charge-carrier trapping of h<sup>+</sup> :



Electron-hole recombination:



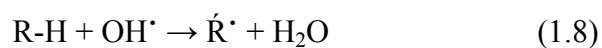
Photoexcited e- scavenging:



Oxidation of hydroxyls:



Photodegradation by  $\text{OH}^\bullet$  :



Direct photoholes:



Protonation of superoxides:



Co-scavenging of  $e^-$  :



Formation of  $\text{H}_2\text{O}_2$ :

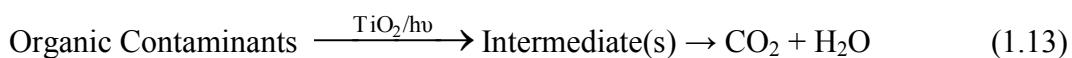


The  $e_{\text{TR}}^-$  and  $h_{\text{TR}}^+$  in Equation 1.4 represent the surface trapped valence band electron and conduction band hole respectively. In this regard, it was found that these trapped carriers are usually bound to the  $\text{TiO}_2$  surface and do not recombine immediately after photo excitation (Furube et al., 2001). The absence of the electron scavengers leads to direct recombination between the photoexcited electron and the valence band hole in nanosecond with simultaneous release of heat energy (Equation 1.5). On the other hand, the presence of electron scavengers like oxygen is important for inhibiting the recombination rate and successful functioning of photocatalytic performance. Equation 1.6 shows how necessary the presence of oxygen is in preventing the direct recombination of electron-hole pair, while allowing the formation of superoxides radical ( $\text{O}_2^{\bullet-}$ ). This  $\text{O}_2^{\bullet-}$  radical would be further protonated to produce the hydroperoxyl radical ( $\text{HO}_2^{\bullet}$ ) and subsequently producing hydrogen peroxide ( $\text{H}_2\text{O}_2$ ) as presented in Equations 1.10 and 1.11 respectively.

However, all these occurrences in photocatalytic reactions are dependant totally on the presence of both dissolved oxygen and water molecules. In fact, without the presence of water molecules, the highly reactive hydroxyl radicals ( $\text{OH}^{\bullet}$ ) could not be generated and impede the photocatalytic reaction of liquid phase organic pollutants (Chong et al., 2010). In other words, the fundamental task of the heterogeneous photocatalyst is to generate free radicals in the solution, mainly the highly reactive hydroxyl radical ( $\text{OH}^{\bullet}$ ), which is traditionally responsible for oxidizing almost all organic pollutants to  $\text{CO}_2$ ,  $\text{H}_2\text{O}$  and simple mineral acids because of its high standard reduction potential of 2.8 V vs. NHE, being exceeded only by fluorine. Thus, during the heterogeneous photocatalytic reactions, the dissolved organic pollutants are degraded to its corresponding intermediates and



subsequently mineralized to carbon dioxide and water, if the photo-treatment time is extended (Equation 1.13) (Chong et al., 2010).



#### 1.4.2 Application of TiO<sub>2</sub>

Apart from its application as pigments, TiO<sub>2</sub> has been studied extensively as photocatalyst. Since 1972, when Fujishima and Honda discovered the photocatalytic splitting of water using TiO<sub>2</sub> electrodes, research on the heterogeneous photocatalysis started growing rapidly (Chen and Mao, 2006). Water splitting is an important application for TiO<sub>2</sub> photocatalysis because hydrogen is a useful material from which to obtain electric energy in fuel cell systems without generating CO<sub>2</sub>. The ability of TiO<sub>2</sub> to oxidize materials can also be used to decompose organic pollutants (Ollis et al., 1991). In the 1980s, detoxification of various harmful compounds in both water and air was demonstrated using powdered TiO<sub>2</sub> as potential purification methods of wastewater and polluted air (Fox and Dulay, 1993; Hoffmann et al., 1995). These results lead to practical applications for water and air purification, such as removal of cigarette smoke and floating fungus. To date, this photocatalyst is widely used in the research of water treatment technology due to its cost competitiveness which is still lower than conventional treatment processes and some other AOPs.

From a practical point of view, alternative photocatalytic materials that are as “versatile, economical, stable, abundant, and non-toxic” as TiO<sub>2</sub> are hard to be found. One of the most viable and practical approaches in developing better photocatalysts is to modify TiO<sub>2</sub> in various methods such as impurity doping, sensitization, surface

modification and integration with other nanostructured materials. As a result, these modifications produced other useful applications of TiO<sub>2</sub> and products related to photocatalysts as shown in Figure 1.4 respectively.



**Figure 1.4:** Applications of TiO<sub>2</sub> (Nakata et al., 2012).

## **1.5 Strategies for improving TiO<sub>2</sub> photoactivity**

Despite of its many potential applications, TiO<sub>2</sub> only absorbs 5 to 8 % energy of the solar spectrum. Hence many works has been adopted for improving the photocatalytic efficiency of TiO<sub>2</sub> towards the visible light response and also in improving the retrieval and reuse of TiO<sub>2</sub> photocatalysts (Pawar et al., 2010; Ibadon and Fitzpatrick, 2013; Park et al., 2013). Herein several conventional approaches are discussed below.

### **1.5.1 Self-sensitization by using colored pollutants**

Organic dyestuffs with visible light absorbing chromophores are responsible for photosensitizing TiO<sub>2</sub> photocatalyst in the field of treating textile wastewater. By this means, the irradiation of adsorbed dye on the TiO<sub>2</sub> surface by visible light leads to the ejection of an electron from the photo-excited dye to the conduction band of TiO<sub>2</sub> photocatalyst. Consequently, the presence of electron scavengers like oxygen leads to the formation of superoxide radical anion, which attacks the dye repeatedly to mineralize it to non-toxic harmless end products (Bauer et al., 2001). The disadvantages of this method come from its limitation for the dyestuff or textile dyes only. The photocatalytic activity that depends basically on the adsorption rate of dyes which is an irreversible process could cause blocking of the active sites on the catalyst surface while higher photocatalytic performance demands for the use of nano scale TiO<sub>2</sub> particles (Nagaveni et al., 2004).

### 1.5.2 Dye modified TiO<sub>2</sub>

Organic dye sensitization has been demonstrated as a useful tool to induce visible light photocatalysis on the surface of TiO<sub>2</sub>. Physical adsorption of dyes occurs through the weak Van der Waals interaction between the dye molecule and the surface of the semiconductor. The mechanism of the dye sensitized photodegradation of pollutants is based on the absorption of visible light for exciting an electron from the highest occupied molecular orbital (HOMO) to the lowest unoccupied molecular orbital (LUMO) of a dye. The excited dye molecule subsequently transfers electrons into the conduction band of TiO<sub>2</sub>, while the dye itself is converted to its cationic radical. The TiO<sub>2</sub> acts only as a mediator for transferring electrons from the sensitizer to the substrate on the TiO<sub>2</sub> surface as electron acceptors, and the valence band of TiO<sub>2</sub> remains unaffected.

In this process, the LUMO of the dye molecules should be more negative than the conduction band of TiO<sub>2</sub>. The injected electrons hop over quickly to the surface of titania where they are scavenged by molecular oxygen to form superoxide radical O<sub>2</sub><sup>•-</sup> and hydrogen peroxide radical •OOH. These reactive species can also disproportionate to give hydroxyl radical. The high photocatalytic performance of the modified TiO<sub>2</sub> photocatalyst is attributed to the photoinjection of an electron from the conduction band of the excited pigment anchored on the photocatalyst particles to the conduction band of the TiO<sub>2</sub> support. Consequently, the quantum yield of the redox process would be increased due to the additional formation of superoxides radical O<sub>2</sub><sup>•-</sup> generated on the TiO<sub>2</sub> conduction band. However, the selected organics dyes are usually not very oxygen-tolerant and not stable enough to realize its sensitizing role.

### **1.5.3 Metal ions modified TiO<sub>2</sub>**

Doping of TiO<sub>2</sub> lattice with a series of metal ions such as V, Cr, Mn, Fe, Ni, etc., causes a red shift in the absorption pattern of TiO<sub>2</sub> photocatalyst. This phenomenon is basically due to the creation of local energy levels of metal ions within the band gap of the TiO<sub>2</sub> photocatalyst. Thus, the electronic properties of the TiO<sub>2</sub> become modified to a large extent and the photocatalyst shows clear response in the visible light region (Anpo and Takeuchi, 2003; Serpone et al., 1994). In fact, the preparation method plays an important role in the photocatalytic efficiency of prepared photocatalyst. Therefore, inserting different types of metal ions into TiO<sub>2</sub> lattice leads to different photocatalytic efficiencies. In some cases there is no photocatalytic activity noticed under visible light and lower activity even in the UV light region compared to non-doped photocatalysts. This retardation in the photocatalytic activity comes from high rate of recombination of charge carriers through the metal ion energy levels (Brezova et al., 1997; Fujishima and Zhang, 2006). Furthermore, doping of metal ions involves other drawbacks related to the thermal instability of the doped TiO<sub>2</sub>, high-cost of ion-implantation facilities, and fast electron trapping by the metal centers (Wang et al., 1999; Yamashita et al., 1998).

### **1.5.4 Doping of TiO<sub>2</sub> with non-metal**

Doping of TiO<sub>2</sub> lattice with non-metal atoms such as N (Kosowska et al., 2005), F (Mrowetz and Selli, 2006), S (Peternel et al., 2006; Periyat et al., 2008) and C (Xiao et al., 2008; Li et al., 2008a) is another widespread technological approach for enhancing the photocatalytic activity of TiO<sub>2</sub> due to the narrowing of its band

gap for larger absorption in the visible light region. For instance, narrowing band gap of N-doped TiO<sub>2</sub> can be achieved by substituting oxygen with nitrogen (N) in the TiO<sub>2</sub> lattice. As a result, the corresponding N (2p) states are centered above the valence band edge. Hence, mixing of N (2p) states with O (2p) states leads to the reduction of the band gap of the N-doped TiO<sub>2</sub> and higher photocatalytic activity for the degradation of color and colorless pollutants can be achieved under visible light irradiation (Kosowska et al., 2005). Additionally, the photocatalytic activity of carbon-doped TiO<sub>2</sub> can be attributed to the presence of oxygen vacancy state between the valence band and conduction band due to the formation of Ti<sup>3+</sup> in the system of carbon-doped TiO<sub>2</sub> (Xiao et al., 2008), or by narrowing the band gap or formed intra-gap localized level (Li et al., 2008b). Even though excellent results can be achieved by applying this modification method, high consumption of energy is required due to the calcination process or heating treatment under specific conditions (Kosowska et al., 2005).

### **1.5.5 Doping TiO<sub>2</sub> with conducting polymer**

Conjugated polymers (CP<sub>s</sub>) with extended  $\pi$ -conjugated electron systems such as polyaniline (PANI), polythiophene, and polypyrrole have shown great promise due to their high absorption coefficients in the visible part of the spectrum, high mobility of charge carriers, and good environmental stability (Pron and Rannou, 2002; Xiong et al., 2007). Furthermore, many CPs in their doped or undoped states are efficient electron donor and good holes transporter upon visible light excitation (Li et al., 2008c). During the past decade, PANI has been the most extensively investigated conducting polymer with good stability, corrosion protection,

nontoxicity, facile and low cost synthesis, and high intrinsic redox properties. In fact, upon irradiation with light, PANI not only is an electron donor but also itself is an excellent hole acceptor (Tan et al., 2004). These special characteristics of PANI make it an ideal material to achieve enhanced charge separation efficiency in the field of photocatalysis (Radhakrishnan et al., 2009).

Combining conducting polymer like PANI, with inorganic semiconductor metal oxides like  $\text{TiO}_2$  has been a topic of great research interest due to their better light and thermal stability, which ensures the recycling of the photocatalysts and it was cheap and easy to synthesize for the commercial scale production as well. In addition, their delocalized conjugated structures are beneficial to rapid photoinduced charge separation and may improve the photocatalytic degradation process. As a result, some groups have used conducting polymers to modify  $\text{TiO}_2$  crystals to improve their performance of solar energy transfer and visible light photoactivity (Liu et al., 2006; Jiang et al., 2008).

## **1.6 Immobilization of $\text{TiO}_2$ photocatalyst**

In heterogeneous photocatalyst technology, there are two major designs of heterogeneous photoreactor systems namely the slurry and immobilized systems (Parra et al., 2004; Kwon et al., 2006). In the slurry system, small  $\text{TiO}_2$  particles such as commercially available Degussa P25 are suspended in the solution to be treated. However, the suspended particles may contaminate the yield and need to be removed. However nano particles are difficult to remove as they stay suspended in water easily, clog filter membranes and penetrate filter materials (Saupe et al., 2005;

Zainal et al., 2005). The filtering of the slurry is therefore not practical and comes with an economic cost.

Thus, immobilization of TiO<sub>2</sub> powder on solid supports is an alternative and convenient method to solve these problems. Although the immobilization of TiO<sub>2</sub> is strongly recommended, the low stability of the immobilized photocatalyst due to the weak attachment of TiO<sub>2</sub> to a carrier has been a fatal problem. Moreover the photocatalytic efficiency of the immobilized TiO<sub>2</sub> system was less than that of the slurry system due to the reduced surface area accessible for photocatalytic reaction as well as low porosity of the supported catalyst layer (Mascolo et al., 2007). Nevertheless immobilized mode photocatalyst can be used for long-term applications without lowering much of its photocatalytic efficiency (Dionysiou et al., 2000; Fabiyi and Skelton, 2000; Jawad and Nawi, 2012). Therefore the catalyst support should be chemically inert in order to avoid any additional source of water pollution coming from the leaching process of any impurities into the treated solution when inorganic adhesives are used as binders for the photocatalyst powder.

## **1.7 ENR/PVC Polymer Blend**

Polymer blends have become a subject of interest in the field of polymeric materials since their individual properties can be modified to obtain desired new properties. The excellent miscibility between ENR50 and PVC is believed to be induced by the highly polar epoxide groups within the ENR50 molecules (Ratnam and Zaman, 1999). PVC is also anticipated to provide high tensile strength and good chemical resistance while ENR can act as a plasticizer for PVC (Peacock and Calhoun, 2006). In general, the preparation of ENR is usually performed by the



epoxidation of NR with peracetic, perbenzoic and perphthallic acids in solution (Hong and Chan, 2004). Epoxidation of natural rubber produces a random copolymer between isoprene and epoxidised isoprene units. The epoxidation process leads to the reduction of the molecular weight of NR with an increase in the density of the ENR produced. ENR has such attractive attributes which indicates that it has oil resistance, reduced air permeability, damping and wet grip comparable to the synthetic specialty rubbers (Perera et al., 2000).

Apart from being renewable, the choice of ENR-50 in this study is based on structural composition of 50 mole % of C=C and epoxide groups respectively, which are randomly distributed in its polymer chain providing sites for physical or chemical interaction. As the mole % epoxidation increases, the rubber becomes much more polar. This means that it will be harder to dissolve in non-polar solvents. Organic solvents such as chloroform, dichloromethane, toluene, xylene, benzene, tetrahydrofuran, dimethylformamide, 1, 2-dimethoxyethane and methylethyl ketone are solvents that ENR can dissolve in.

Polyvinyl chloride, commonly abbreviated PVC, is the third most widely produced plastic, after polyethylene and polypropylene. PVC is used in construction because it is more effective than traditional materials such as copper, iron or wood in pipe and profile applications. Pure polyvinyl chloride is a white, brittle solid. It is insoluble in alcohol, but soluble in dichloromethane. In fact, the mechanical properties of ENR50/PVC have been widely studied and reported in the literatures (Ratnam et al., 2001). Studies have shown that stabilised or plasticised PVC and ENR forms miscible blends at any ratio, both in the uncrosslinked or crosslinked stage Perera et al., 2001 in which PVC is expected to impart high tensile strength and good chemical resistance while ENR acts as a permanent plasticiser for

PVC, induce good tear strength and enhance resistance against hydrocarbon oils. At low mixing temperatures, agglomeration of PVC particles and the incomplete dissociation of PVC grains were both observed (Ratnam and Zaman, 1999). However, at high mixing temperatures, due to improved melting and fusion of PVC, individual primary particles and distinct interfaces were not observed. Self crosslinkable blends were also reported to be formed during high temperature mouldings which are found to be immiscible (Perera et al., 2001).

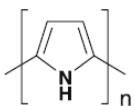
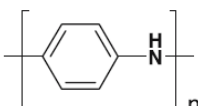
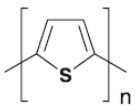
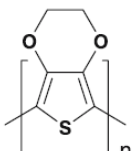
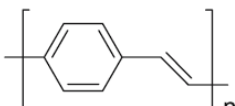
## **1.8 Polyaniline (PANI)**

Among the conducting polymers, polyaniline is emerging as the material of choice for many applications. Polyaniline (PANI) is one of the most important conducting polymer that possess excellent electronic, optical, and redox properties and environmental stability. The thermal stability of PANI is superior to other ionic conducting polymers (ICPs) (Table 1.1). The processability and conductivity of PANI are also fairly good. From economic point of view, PANI is favourable than other ICPs because the aniline monomer is less expensive than other monomers used (Blinova et al., 2007). Moreover preparation of PANI is simple while it also has adjustable properties and numerous application possibilities.

PANI was initially discovered in 1834 by Runge, and it was referred to as aniline black (Kang et al., 1998). Following this, Letheby carried out research to analyse this material in 1862. Then, Green and Woodhead found the different stages of oxidation level of PANI which contributed various characteristic properties. Moreover, Diaz and Logan,(1980) discovered this interesting characteristic of polyaniline dealt with its electrical conductivity and other properties like electro-chemical redox activity and reversible doping/dedoping. PANI is a phenylene based

polymer having–NH– group on either side of the phenylene ring. The oxidation and reduction takes place on this–NH– group, and various forms are obtained due to the number of imine and amine segments on the PANI chain. Aniline basically undergoes oxidative polymerization in the presence of a protonic acid (Dionysiou et al., 2000).

**Table 1.1:** Chemical structures of typical conjugated polymers

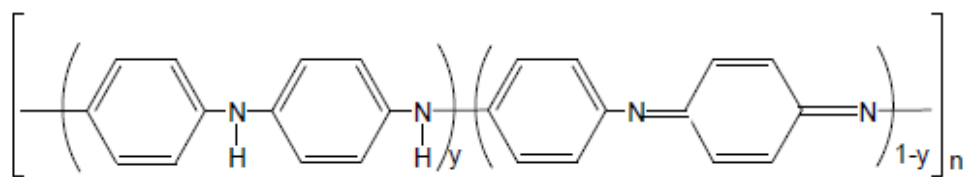
Name	Structure
Polypyrrole	
Polyaniline	
Polythiophene	
Poly(3,4-ethylenedioxythiophene)	
Poly(para-phenylene vinylene)	

Polyaniline has been reported to have the following idealised structure as shown in Figure 1.5a (Sniechowski, 2005). The average oxidation state ( $y$ ) could varied in different oxidation state depending on the preparation method which are a fully reduced form (leucoemeraldine), partially reduced form (emeraldine), and fully oxidized form (pernigraniline) respectively. The level of oxidation state of PANI can be determined based on the colour of the prepared PANI. Table 1.2 shows the colors of each five oxidation state of PANI. The terms “leuco-emeraldine,” “emeraldine,” and “pernigraniline” refer to the different oxidation states of the polymer where (1-

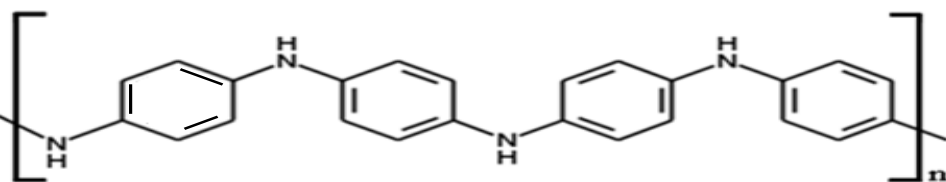
$y = 0, 0.5, \text{ and } 1$ , respectively, either in the base form, e.g., emeraldine base, or in the protonated salt form, e.g., emeraldine hydrochloride. Leucoemeraldine base (fully reduced) is very reactive. It reacts even with minute amount of oxygen and they are environmentally unstable. Emeraldine base (partially oxidized) is environmentally stable and does not undergo any change in chemical structure on prolonged storage. Pernigraniline base (fully oxidized) is also environmentally stable and further oxidation is not possible with fully imine groups. The fully oxidized and fully reduced state of PANI is not in a conducting state. The most desirable oxidation state is emeraldine salt (PANI-ES). PANI-ES prepared by the oxidative polymerization of aniline exists in two chemical forms, a protonated PANI and PANI base. Polyaniline is protonated in acidic media; it is green or dark green. In this study, works had been focused on the oxidized state of emeraldine PANI due to its stability and conducting properties.

**Table 1.2:** The colors of each oxidation state of PANI.

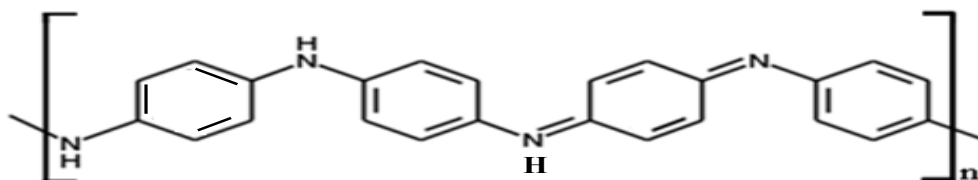
PANI condition	oxidation state	Color
Leucoemeraldine	$y = 1$	pale yellow or colorless
Protoemeraldine	$y = 0.75$	light green
Emeraldine	$y = 0.5$	green or darkgreen
Nigraniline	$y = 0.25$	blue or darkblue
Pernigraniline	$y = 0$	Violet



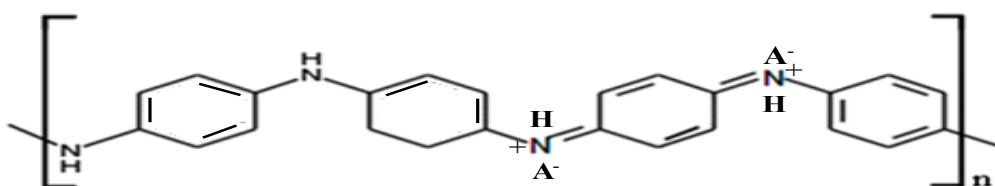
(a)



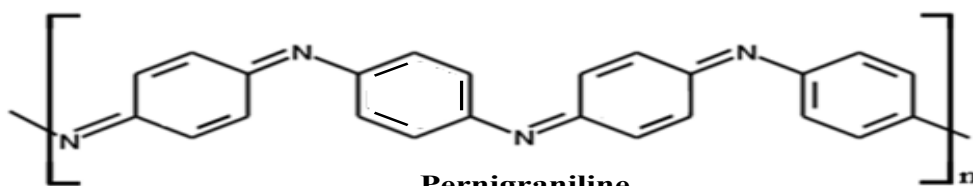
**Leucoemeraldine**



**Emeraldine base**



**Emeraldine salt**



**Pernigraniline**

(b)

**Figure 1.5:** The general structure of (a) PANI and (b) The chemical structures of four oxidation states of polyaniline (Sharma, 2006).

## **1.9 Method of PANI synthesis**

Based on the literature review, there are many different ways to produce PANI such as chemical, electrochemical, template, enzymatic, photo, and a number of other special methods. The most common used is chemical polymerization which has being subdivided into heterophase, colloidal dispersion, emulsion, solution, interfacial, seeding, metathesis, self-assembling, and sonochemical polymerizations.

### **1.9.1 Synthesis of polyaniline colloidal dispersion**

PANI is typically produced by the oxidative polymerization of aniline in an acidic aqueous medium and is obtained as a precipitate (Stejskal and Gilbert, 2002) . If a suitable water-soluble polymer such as poly(N-vinylpyrrolidone) (PVP) is added to the reaction mixture, colloidal PANI particles are formed instead of precipitation. Such a process is known as dispersion polymerization (Barrett, 1975; Palaniappan and John, 2008). Several characteristics of this process are as follows: (a) The monomer is soluble in the reaction medium; (b) the produced polymer is insoluble under the same conditions; and (c) its macroscopic precipitation is prevented by the presence of the so-called steric stabilizer. Hence, such colloids are called dispersions. The colloidal PANI particles have a typical average size of a few tens to hundreds of nanometers and are thus often regarded as nanocolloids (Gurunathan and Trivedi, 2000; Blinova et al., 2005). The shape of the particles may be spherical, globular, granular, cylindrical or branched dendritic structures (Stejskal and Gilbert, 2002; Stejskal et al., 2003; Li et al., 2008c; Bilal et al., 2012).

### **1.9.2 Direct and inverse emulsion polymerization of aniline**

In the emulsion polymerization, the monomer is dispersed in an aqueous phase to form a uniform emulsion. The emulsion is stabilized by a surfactant and the polymerization reaction is carried out (Gowariker et al., 1986; Murugesan et al., 2004; Palaniappan and Amarnath, 2005; Palaniappan and John, 2005; Li et al., 2013). For the synthesis of PANI by emulsion polymerization, aniline along with a protonic acid and an oxidant are combined with a mixture of water and a nonpolar or weakly polar solvent, for example, xylene, chloroform, or toluene (sparingly soluble or insoluble in water). In some instances, in order to form an emulsion with the above systems, a protonic acid such as dodecylbenzene sulfonic acid is employed, which has a substantial emulsifying ability in weakly polar solvents. In addition, the product of the above reaction cannot be isolated directly, since the PANI salt exists in the emulsion along with other by-products. In most cases, the product is isolated by destabilizing the emulsion through the addition of acetone. The PANI salt is then collected and subjected to repeated washing to free it from other constituents (Österholm et al., 1994; Kinlen et al., 1998; Yan and Xue, 1999; Yavuz and Gök, 2007).

With the progress in the development of PANI, different types of emulsions have been prepared for PANI synthesis and accordingly the synthesis methods have different names. The inverse emulsion polymerization process involves the formation of an aqueous solution of the monomer aniline, which is emulsified in a nonpolar organic solvent, for example chloroform, isooctane, toluene, or in a mixture of solvents (Grigoras et al., 2008). The polymerization is then initiated with an oil-soluble initiator such as ammonium persulfate (APS), benzoyl peroxide, and so on (Palaniappan and Sairam, 2008). The physical state of the inverse emulsion system